π-Conjugated Molecules Crosslinked Graphene-Based Ultrathin Films and Their Tunable Performances in Organic Nanoelectronics

Xiaowei Ou, Penglei Chen, Lang Jiang, Yunfan Shen, Wenping Hu,* and Minghua Liu**

Graphene-based ultrathin films with tunable performances, controlled thickness, and high stability are crucial for their uses. The currently existing protocols, however, could hardly simultaneously meet these requirements. Using amino-substituted π-conjugated compounds, including 1,4-diaminobenzene (DABNH2), benzidine (BZDNH2), and 5,10,15,20-tetrakis (4-aminophenyl)-21*H*,23*H*-porphine (TPPNH2), as cross-linkages, a new protocol through which graphene oxide (GO) nanosheets can be anchored on solid supports with a high stability and controlled thickness via a layer-by-layer method is presented. A thermal annealing leads to the reduction of the films, and the qualities of the samples can be inherited by the as-produced reduced GO films (RGO). When RGO films are integrated as source/drain electrodes in OFETs, tunable performances can be realized. The devices based on the BZDNH2-crosslinked RGO electrodes exhibit similar electrical behaviors as those based on the non-π-conjugated compound crosslinked electrodes, while improved performances can be gained when those crosslinked by DABNH2 are used. The performances can be further improved when RGO films crosslinked by TPPNH2 are employed. This work likely paves a new avenue for graphene-based films of tunable performances, controlled thickness, and high stability.

1. Introduction

Graphene oxide (GO) has currently received much attention as one of the most frequently investigated graphene cousins.[1] This is owing to its fascinating basal plane and edge, wherein various oxygen-containing groups are decorated, facilitating functionalization of graphene materials.[1] Numerous GO-based advanced devices in energy conversion/storage, sensors, nanoelectronics, and so forth, have thus far been developed.[1,2] To realize these applications, GO should be organized to form ultrathin films simultaneously featured with high stability, controlled thickness, and tunable performances. An ultrathin GO film at the nanometer level could endow the samples with an excellent optical transmittance,[3] which is essentially required to achieve high-performance nano-optoelectronics, although a thicker thickness (which would decrease the optical transmittance) favors an improvement in film conductance. A controlled thickness within the nanometer level could provide significant scientific forums for their layer-number-dependent physicochemical properties, a tunable performance could endow them with fertile opportunities for desired uses, while a high stability is strongly desired for the practical applications to withstand the multi-step post-production process, all of which are essentially required for high-quality graphene films of practical uses.

Thus far, GO-based films have been successfully integrated by various methods, including spin coating, layer-by-layer (LBL) assembly, Langmuir-Blodgett (LB) technique, electrophoretic deposition, spray deposition, drop casting, evaporation-induced self-assembly, and so forth.[3–8] For example, GO nanosheets could be deposited on solid supports via the sophisticated LB technique,[5c,5d,6a] while the excellent dispersibility of GO in water (subphase) makes it difficult for practical operations and, at the same time, an LB trough has to be employed during such assembly. On the other hand, GO nanosheets could also be organized to form multilayer films with tunable thickness through LBL assembly.[5b,6c,6e,8] However, owing to the non-covalent interactions (electrostatic interactions or hydrogen-bonding) between the interlayers, the as-formulated non-covalent films are easy to disassembly.[9] In the cases of spin coating, spray deposition, drop casting, evaporation-induced self-assembly, and so on, GO films could be assembled facilely over large area surface.[3,5a,6b,6d,6f,7] Nevertheless, the thickness of such films could not be well controlled at a lever of a few nanometers over large area surface, and meanwhile the formulation of these films have to be carried out with great cautions in order to produce GO-based films

Dr. X. Ou, Dr. P. Chen, Dr. L. Jiang, Ms. Y. Shen, Prof. W. Hu, Prof. M. Liu
Beijing National Laboratory for Molecular Sciences
Institute of Chemistry
Chinese Academy of Sciences
Beijing, 100190, P. R. China
E-mail: chenpl@iccas.ac.cn; cpl@zzu.edu.cn; huwp@iccas.ac.cn; liumh@iccas.ac.cn
Dr. P. Chen, Ms. Y. Shen
College of Chemistry and Molecular Engineering
Zhengzhou University
100 Science Road, Zhengzhou, Henan, 450001, P. R. China

DOI: 10.1002/adfm.201302153

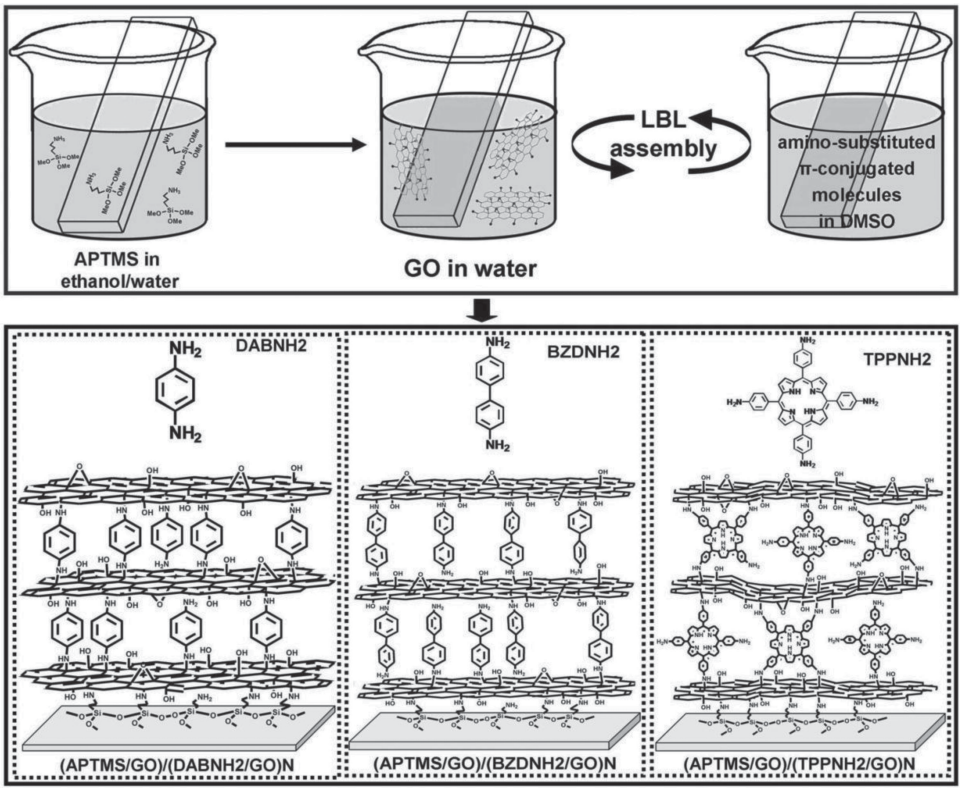

Scheme 1. An illustration for the fabrication of GO films crosslinked by amino-substituted molecules of different π-conjugated systems via a LBL method. To obtain the corresponding RGO films, the original formulated samples were treated by a thermal annealing. The drawings are not to scale.

with good reproducibility. In most cases, the manufactured GO films were simply stuck to but not anchored on the solid supports, endowing them with less stability. It thus can be seen that although GO-based ultrathin films could be constructed by various protocols, they could hardly meet the above-mentioned significant requirements (high stability, controlled thickness, and tunable performances) simultaneously, which are of paramount importance for the practical uses of GO.[3–8]

We recently developed a covalent LBL protocol for graphene-based films.[9a] Using (3-aminopropyl) trimethoxysilane (APTMS) as cross-linkage, GO and reduced GO (RGO) films (APTMS/GO)N and (APTMS/RGO)N with high stablity, were fabricated. However, APTMS itself is electronically inactive, contributing only to the high stability of the films but not to their function performances. It still remains a formidable challenge to construct graphene-based films simultaneously featured with high stability, controlled thickness, and tunable performances. As known, owing to their delocalized electrons, which offer conductive pathway along their skeleton, π-conjugated molecules have attracted great concerns as active species in organic nanodevices.[10] This inspires us to ask if graphene-based films simultaneously characterized with high stability, controlled thickness, and tunable performances could be formulated when π-conjugated covalent linkages are used? How the π-conjugated systems of these linkages could affect the performance of the films?

To tackle these formidable challenges and to answer these significant questions, we herein report our new findings that high-quality GO ultrathin films, simultaneously featured with controlled thickness, tunable performances and high stability as well, could be assembled via a new covalent LBL protocol, wherein amino-substituted compounds of different π-conjugated systems, 1,4-diaminobenzene (DABNH2), benzidine (BZDNH2), and 5,10,15,20-tetrakis (4-aminophenyl)-21*H*,23*H*-porphine (TPPNH2), are used as linkages, as shown in **Scheme 1**. After a thermal annealing, the obtained RGO films retain the qualities of their parent films. Compared with the OFETs using (APTMS/RGO)/(APTMS/RGO)N as electrodes, those based on (APTMS/RGO)/(BZDNH2/RGO)N show approximately similar performances, while those based on (APTMS/RGO)/(DABNH2/RGO)N exhibit distinctly improved performances. Significantly, the performance of our devices could be further improved evidently when (APTMS/RGO)/(TPPNH2/RGO)N films are employed. The use of dual functional linkages, namely, the linkage serves not only as an impact bridge for the high stability and controlled thickness of graphene-based ultrathin films; more importantly, as a modulator for their tunable performance, our new protocol has broad opportunities not only for the next generation graphene-based high-performance organic nanoelectronics, but also for graphene films of other desired motives in terms of using elaborately-designed linkages of desired functions or properties.

2. Results and Discussion

As illustrated in Scheme 1, to fabricate covalently crosslinked GO films using DABNH2, BZDNH2, or TPPNH2 as the

cross-linkages, solid substrates of a hydroxylated surface was first aminated with APTMS, onto which GO nanosheets were grafted via the chemical reaction between the amino groups of APTMS and the epoxy groups of GO.[9a] To make a clear description, thus formulated samples, which will be used as the sublayer for the construction of the π-conjugated molecules crosslinked GO films, are designated as (APTMS/GO). Subsequently, thus-formulated substrates, whose surface was covalently grafted with GO nanosheets, were immersed in an aqueous dispersion of GO and a DMSO solution of our π-conjugated cross-linkages alternately and consecutively. The as-assembled samples are named as (APTMS/GO)/(DABNH2/GO)N, (APTMS/GO)/(BZDNH2/GO)N, and (APTMS/GO)/(TPPNH2/GO)N, respectively, when DABNH2, BZDNH2, and TPPNH2 are used as the interlayer cross-linkages.

To monitor the LBL assembly process, the real-time UV-vis spectra of the films were measured using the UV-vis spectrum of the (APTMS/GO) sublayer as baseline, as shown in Figure S1, Supporting Information. For (APTMS/GO)/(DABNH2/GO)N, there exists a good linear correlation between the number of bilayers *N* and the intensity of the absorptions of GO at ≈231 nm (Supporting Information, Figure S1A1,A2). In the cases of (APTMS/GO)/(BZDNH2/GO)N (Supporting Information, Figure S1B1,B2) and (APTMS/GO)/(TPPNH2/GO)N (Supporting Information, Figure S1C1,C2), almost similar results are obtained. These observations basically suggest that GO nanosheets could be sucessfully grafted on the (APTMS/GO) sublayer uniformly and reproducibly using our amino-substituted π-conjugated molecules as the cross-linkages. Note that besides the GO absorption located at ≈231 nm, a distinct absorption located around 436 nm, whose intensity increases linearly with the number of bilayers *N*, could also be distinctly observed from the samples of (APTMS/GO)/(TPPNH2/GO)N. This band could be ascribed to the Soret-band of our porphyrin TPPNH2.

The FT-IR spectra of the as-prepared films and those of the original GO powders and the (APTMS/GO) sublayer were investigated, as shown **Figure 1**. For the original powdery GO nanosheets (Figure 1, curve A), it can be seen that two bands at 1628, 1730 cm^{-1}, together with a broad band at ≈3400 cm^{-1}, which are attributed to vibrations of the adsorbed water molecules and the skeletal vibrations of the un-oxidized graphitic domains, the C=O carbonyl stretching, and O–H stretching of C–OH, respectively, are detected.[11] At the time, distinct peaks at approximately 990, 1049, and 1230 cm^{-1}, ascribing to the typical epoxy vibrations, and C–O vibrations of the epoxy (C–O–C) and C–OH units, respectively, could also be detected.[11,12]

In the case of the (APTMS/GO)/(DABNH2/GO)3 films (Figure 1, curve C1), several vibrations located at ≈3320, 3210 and 1636, 1525 cm^{-1}, which are attributed to the asymmetric and symmetric N–H stretching, and scissoring and bending vibrations of N–H, respectively, could be observed.[13] These results indicate that our DABNH2 molecules are successfully integrated in the formulated LBL films. In these films, the above-mentioned broad band around ≈3400 cm^{-1} (O–H stretching of C–OH) and the peak at ≈1730 cm^{-1} (the C=O carbonyl stretching) of the original GO nanosheets could also be detected distincly, suggesting the inclusion of GO nanosheets in the films. At the same time, several bands at ≈1080 and 2854, 2921 cm^{-1}, which could be assinged to the asymmetric

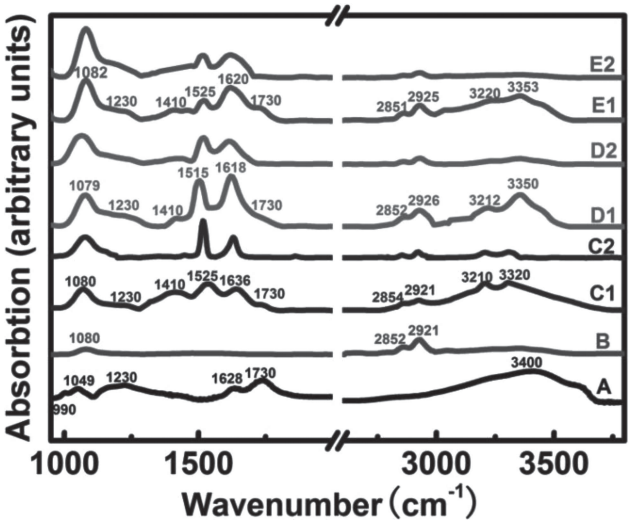

Figure 1. FT-IR spectra of our original GO powders (A) and the (APTMS/GO) sublayers (B), and those of the LBL films of (C1,C2) (APTMS/GO)/(DABNH2/GO)3, D1,D2) (APTMS/GO)/(BZDNH2/GO)3, and E1,E2) (APTMS/GO)/(TPPNH2/GO)3 before (C1,D1,E1) and after (C2,D2,E2) the thermal annealing treatment.

stretching of Si–O–Si, and symmetric and antisymmetric vibration of CH_2, respectivley, are observed. This is owing to the existance the covalent cross-linkage APTMS in the sublayer of the films.[9a] It has been shown that the dissociation of water molecules would possibly form C–H bond at the defects of graphene lattice and contribute to the FT-IR band around 2921 cm^{-1}.[14] While we cannot exclude such possiblity, this band could mainly be attributed to the APTMS linkages located at the sublayer, since APTMS has three methylene groups on its molecular skeleton.[9a] Actually, the presence of C–H group is an important issue, because it could influence the performance of graphene-based optoelectronic and plasmonic devices,[15a–15d] especially at the contacts with metal electrodes.[15d,15e]

Compared with the FT-IR spectra of the (APTMS/GO) sublayer (Figure 2, curve B), the vibration band of Si–O–Si at ≈1080 cm^{-1} of our (APTMS/GO)/(DABNH2/GO)3 films manifests itself as a more evident peak with relatively higher intensity, while the CH_2 vibrations at ≈2854, 2921 cm^{-1} display negligible changes. These experimental facts indicate the formation of secondary amino units in our LBL films, which could also display vibrations at ≈1080 cm^{-1} (the C–N stretching band of the secondary amino group).[16] Meanwhile, it is noteworthy that the vibrations related to the epoxy units (990, 1049, and 1230 cm^{-1}) of GO could not be evidently discerned from the FI-TR spectrum of our (APTMS/GO)/(DABNH2/GO)3 films. These experimental results strongly suggest the sucessful chemical reaction between the amino groups of our DABNH2 molecules and the epoxy groups of the GO nanosheets during the LBL assembly process, resulting in the formation of covalent bonds between the GO interlayers, as schematically illustrated in Scheme 1.

Besides, a peak around ≈1410 cm^{-1}, ascribing to the symmetrical stretching vibrations of carboxylate anion $\nu(COO^-)$,[17] is also detected from the formulated films. This peak of

carboxylate anion is not observed distinctly from the FT-IR spectrum of the original powdery GO nanosheets. This fact indicates that, in addition to the formation of covalent bonds with the epoxy groups of GO, some of the -NH_2 groups of DABNH2 could also interact with the -COOH groups of GO nanosheets, resulting in an formation of carboxylate anions. As shown in Figure 1 (curves D1 and E1), approximately similar spectral features could be observed from the FT-IR spectra of the (APTMS/GO)/(BZDNH2/GO)3 and (APTMS/GO)/(TPPNH2/GO)3 films, indicating that LBL films with covalent features could also be formulated when BZDNH2 and TPPNH2 molecules are employed as the interlayer cross-linkages.

Experimentally, several dozens of samples were fabricated, and we found that the as-constructed LBL films could display good reproducibility. This is different from the LBL GO films integrated via the electrostatic interactions, wherein the reproducibility of samples depends greatly on the practical operations, especially, the rinsing of the non-covalent films should be carried out carefully to obtain samples reproducibly as much as possible.[9a] As shown in Figure S2 (Supporting Information), only slight changes could be observed from the UV-vis spectra of the (APTMS/GO)/(DABNH2/GO)4, (APTMS/GO)/(BZDNH2/GO)4 and (APTMS/GO)/(TPPNH2/GO)4 films, after these samples are ultrasonicated thoroughly in a water bath for 5 h, indicating their high stability. This is also essentially different from the LBL films of GO constructed by means of electrostatic interactions, which disassembly immediately upon an ultrasonication treatment of only 20 min.[9a] Accompanied by the above-mentioned facts of the FT-IR spectra, these experimental result further indicate the covalent feature of our as-assembled films, leading to their excellent reproducibility and high stability.[18]

The thickness of our films was investigated by means of AFM measurements, as shown in Figure S3, Supporting Information. For the (APTMS/GO)/(DABNH2/GO)1 films (Supporting Information, Figure S3A1), wherein a 1 bilayers film of (DABNH2/GO) was covalently grafted on a (APTMS/GO) sublayer, an averaged thickness of ≈2.6 nm is obtained. Considering that the averaged thickness of the 1 bilayers film of (APTMS/GO) evaluated by AFM measurements is ≈1.4 nm,[9a] a thickness of ≈1.2 nm could be deduced for a 1 bilayers film of (DABNH2/GO). This data is larger than the ≈0.8 nm thickness of the GO nanosheets.[11a,19] This is owing to the spacer effect brought out by the DABNH2 cross-linkages, which are intercalated between the GO interlayers, as illustrated in Scheme 1. As shown in Figure S3 (Supporting Information, panels A2–A5), an averaged thickness of ≈3.7, 4.7, 6.0, and 7.0 nm could be obtained, respectively, when the number of the (APTMS/GO)/(DABNH2/GO)N films *N* is increased to 2, 3, 4, and 5. As indicated in Figure S3 (Supporting Information, panel A6), the number of the bilayers *N* and the averaged films thickness displays a good linear correlation, wherein an increment of ≈1.1 nm could be derived. This value is very close to the thickness of a 1 bilayers film of (DABNH2/GO), suggesting that using our amino-substituted π-conjugated molecule DABNH2 as the interlayer cross-linkages, GO multilayer films with a controlled thickness could be easily formulated in an LBL manner.

As shown in Figure S3 (Supporting Information, panel B1-B5), in the cases of the (APTMS/GO)/(BZDNH2/GO)N films, almost similar results are observed except that an increment of ≈1.5 nm in the averaged film thickness could be derived from the linear correlation between the number of the bilayers *N* and the averaged thickness of the films. This data is larger than that of the above-mentioned (APTMS/GO)/(DABNH2/GO)N films, which is owing to the longer molecular skeleton of the BZDNH2 species. These results suggest that when BZDNH2 is employed as the interlayer covalent cross-linkage, GO nanosheets could also be organized to form multilayered films with a controlled thickness. As shown in Figure S3 (Supporting Information, panel A1–A5 and B1–B5), when the number of the bilayers *N* is 1, 2, 3, 4, and 5, respectively, the root-mean-square (rms) roughness (*R*q) of the (APTMS/GO)/(DABNH2/GO)N films is estimated to be ≈1.12, 1.60, 1.97, 2.34, and 4.16 nm, and in the cases of the (APTMS/GO)/(BZDNH2/GO)N films, this data is estimated to be ≈1.73, 2.42, 2.90, 3.87, and 6.62. These results are approximately at the same level as those of the corresponding (APTMS/GO)/(APTMS/GO)N LBL films, which are crosslinked by APTMS.[9a] Together with the results of UV-vis spectra presented in Figure S1 (Supporting Information, panels A1, A2, B1, and B2), these facts indicate that our LBL films, which are crosslinked by π-conjugated compounds DABNH2 and BZDNH2, probably have a nice layered structure.

To confirm this proposal, the XRD spectra of our films were measured, as shown in **Figure 2**. In the case of the (APTMS/GO)/(DABNH2/GO)15 films, an evident diffraction peak (2θ) at ≈14.2° could be observed (Figure 2, curve A1). Considering the aforementioned results of AFM investigations, this peak could be attributed to the second order diffraction peak of the films, wherein an interlayer distance of ≈1.2 nm could be deduced. This data is very close to the thickness increment of these films

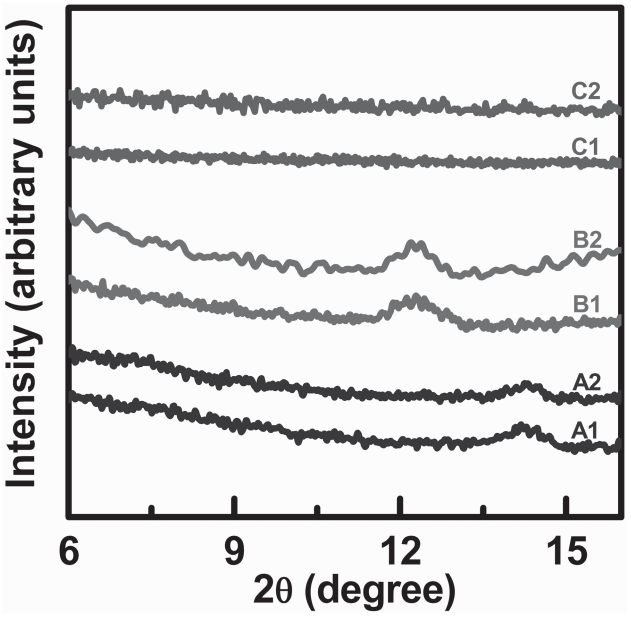

Figure 2. XRD pattern of the (APTMS/GO)/(DABNH2/GO)15 (A1 and A2), (APTMS/GO)/(BZDNH2/GO)15 (B1 and B2), and (APTMS/GO)/(TPPNH2/GO)15 (C1 and C2) films before (A1, B1 and C1) and after (A2, B2, and C2) the thermal annealing treatment.

estimated by AFM measurements (Supporting Information, Figure S3, panels A1–A6), clearly confirming that the as-formulated films have a layered structure, wherein single layered DABNH2 molecules are successfully intercalated between the GO interlayers, as shown in Scheme 1. On the other hand, a diffraction peak at ≈12.3° could be observed obviously from the XRD pattern of the (APTMS/GO)/(BZDNH2/GO)15 films (Figure 2, curve B1), wherein an interlayer distance of ≈1.4 nm could be derived, suggesting that the films also have a layered structure. This value is approximately similar to the averaged thickness of the (BZDNH2/GO) bilayers obtained from AFM investigations (Supporting Information, Figure S3, panel B1–B6), and at the same time, it is apparently larger than that of the (APTMS/GO)/(DABNH2/GO)N films. This is in good agreement with the facts observed from AFM measurements, wherein the comparatively larger interlayer distance of the (APTMS/GO)/(BZDNH2/GO)N films could be owing to the longer molecular skeleton of the BZDNH2 species.

As shown in Figure 2 (curve C1), no diffraction peaks could be evidently observed from the XRD pattern of the (APTMS/GO)/(TPPNH2/GO)N films, indicating that the organized films in this case have a poor layered structure. The AFM images of these films were measured as shown in the Supporting Information (Figure S3, panels C1-C5). In can be seen that the rms roughness of the films is estimated to be ≈3.56, 4.76, 6.35, 7.83, and 10.14 nm, when the number of the bilayers *N* is 1, 2, 3, 4, and 5, respectively. These data are larger than those of the corresponding data obtained in the cases of the (APTMS/GO)/(DABNH2/GO)N and (APTMS/GO)/(BZDNH2/GO)N films. These experimental facts suggest that compared with their counterparts crosslinked by DABNH2 and BZDNH2, the films assembled using TPPNH2 as the cross-linkage have a more uneven surface.

On one hand, there are four amino groups at the four corners of the TPPNH2. On the other hand, the epoxy groups of GO nanosheets are distributed arbitrarily but not regularly on the basal plane of GO. Thus, the TPPNH2 molecules could crosslink stochastically with the interlayer GO nanosheets via the opposite amino groups, or via the neighboring amino groups (Scheme 1), leading to poor layered structure with a rough surface. Nevertheless, it can be seen from the AFM images of the samples that an averaged film thickness of ≈3.6, 6.0, 7.9, 11.3, and 12.4 nm could be obtained when the number of the bilayers *N* is increased from 1, 2, 3 to 4 and 5, respectively. As plotted in the Supporting Information (Figure S3, panel C6), a linear correlation between the averaged film thickness and the number of the bilayers *N* could be obtained. On the basis of this plot, an increment of ≈2.2 nm in the film thickness could be derived, suggesting that the film thickness in this case could also be controlled approximately.

It can be seen from the above results that using amino-substituted molecules of different π-conjugated systems as the cross-linkages, ultrathin GO films with high stability, controlled number of GO layers could be covalently crosslinked over large area surface. Considering the fertile functions of π-conjugated molecules, especially their general concerns in organic nanoelectronics,[10] the as-assembled GO films endow us with good opportunities to investigate their electrode applications in OFETs, wherein the effect of the different π-conjugated systems might be disclosed. Before the integration of these covalent LBL films into nanodevices, an annealing induced reduction of the films was carried out first. As shown in Figure S4 (Supporting Information), the absorption of the unreduced GO nanosheets originally located at ≈231 nm display a bathochromic shift of ≈36 nm to ≈267 nm after the annealing, indicating a successfully reduction of the films,[20] which leads to the formation of the corresponding RGO films, (APTMS/RGO)/(DABNH2/RGO)N, (APTMS/RGO)/(BZDNH2/RGO)N and (APTMS/RGO)/(TPPNH2/RGO)N. Similar as what we have found from the corresponding films before the annealing (Figure S1, Supporting Information), the intensity of the absorption of RGO nanosheets at ≈267 nm increases linearly with the number of bilayers *N* (Figure S4, Supporting Information), preliminarily indicating that our films might maintain their structural features during the annealing procedure.

To verify the successful reduction, Raman spectra of these samples before and after the thermal annealing were measured. As shown in Figure S5 (Supporting Information) a *D*-band at ≈1348 cm^{-1} and a *G*-band at ≈1598 cm^{-1}, which are typical Raman features of GO nanosheets, are observed from the Raman spectra of the original formulated LBL films before the thermal annealing treatments.[21,22] In these cases, the relative intensity of *G*-band is higher than that of *D*-band. In contrast, the intensity ratio between the *G*-band and *D*-band (I_G/I_D) exhibits an evident decrease after the annealing treatment. Accompanied by the facts observed from the UV-vis spectra, these results further indicate the achievement of the reduction of the films and the formation of RGO-based films.[21,22]

The AFM images of the films after the annealing treatments were measured, as shown in Figure S6 (Supporting Information). In the cases of the (APTMS/RGO)/(DABNH2/RGO)N films, their rms roughness is estimated to be ≈0.89, 1.45, 1.85, 2.01, and 3.70 nm, when the number of the bilayers *N* is 1, 2, 3, 4, and 5, respectively. These values are smaller than those of the corresponding films before the annealing treatment. For the (APTMS/RGO)/(BZDNH2/RGO)N and (APTMS/RGO)/(TPPNH2/RGO)N films, similar annealing-induced roughness improvement phenomena have been observed. This could be owing to the elimination of oxygen-containing groups and graphitization of the sample caused by the annealing induced reduction.[23] As indicated in Figures S3,S6 (Supporting Information), compared with corresponding original films before the annealing treatment, the samples display negligible changes in their averaged thickness after the annealing, and the linear correlation between the number of the bilayers *N* and the averaged film thickness could still be observed. These facts further suggest that our LBL films could preserve their structural characters after the reduction. To solidly confirm these proposals, the XRD spectra of these RGO films were investigated. As presented in Figure 2, the XRD pattern of our samples display negligible changes after the annealing induced reduction, solidly confirming that the covalent films could truly retain their structural features after the reduction.

It thus could be proposed that the resultant RGO films might hold their covalent characters, which is very important to ensure their stability. To validate this, the RGO films (APTMS/RGO)/(DABNH2/RGO)4, (APTMS/RGO)/(BZDNH2/RGO)4 and (APTMS/RGO)/(TPPNH2/RGO)4 were ultrasonically

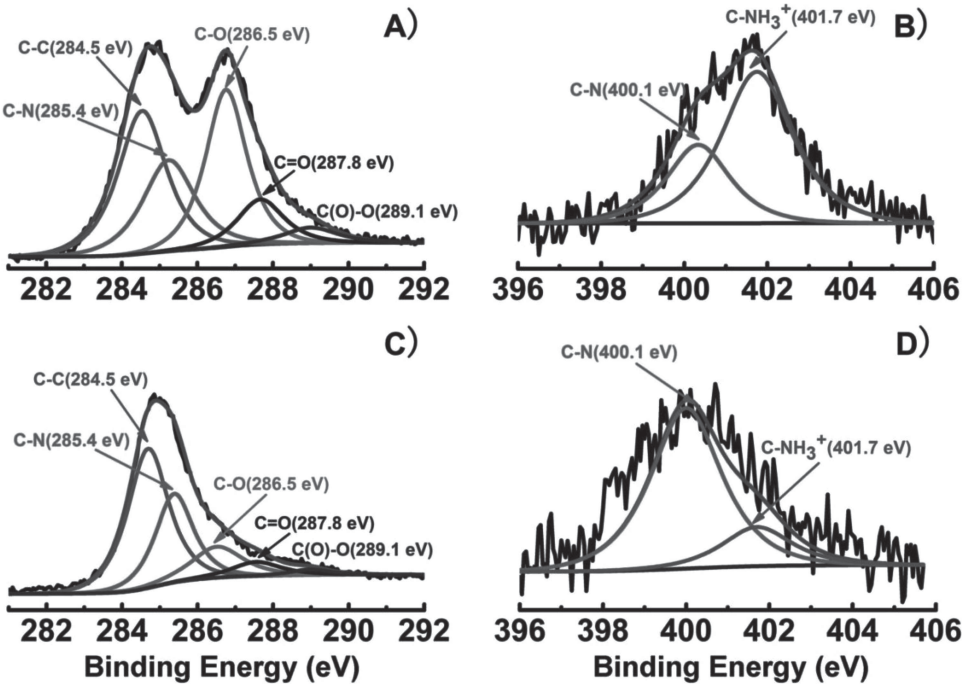

Figure 3. A,C) C1s and B,D) N1s XPS spectra of the (APTMS/GO)/(DABNH2/GO)5 films before (A,B) and after (C,D) the thermal annealing treatments. See Supporting Information, Figures S7,S8, for those of the (APTMS/GO)/(BZDNH2/GO)5 and (APTMS/GO)/(TPPNH2/GO)5 films, respectively.

treated in water bath adequately for 5 h, after which their UV-vis spectra were measured. As shown in Figure S2 (Supporting Information, panels A2, B2, C2), it can be seen that the samples exhibit negligible changes in their UV-vis spectra after an ultrasonication treatment of 5 h. This phenomenon is substantially different from that of the RGO LBL films fabricated via the electrostatic interactions, which exhibits a distinct disassembly after an ultrasonication treatment of only 20 min.[9a] In contrast, this result is similar to what we have observed from the originally fabricated GO-based films (Supporting Information, Figure S2, panels A1, B1, C1), indicating that their high stability could be inherited after the reduction, and that the interlayers of these RGO-based films might still be covalently linked via our π-conjugated cross-linkages.[18]

To further verify this suggestion experimentally, the FT-IR spectra of our RGO films were investigated. As shown in Figure 1, the most distinct changes in the FT-IR spectra of all of the films after the thermal annealing are that the O–H stretching of C–OH around 3400 cm^{-1}, the C=O carbonyl stretching at ≈1730 cm^{-1}, the symmetrical stretching vibrations of carboxylate anion $\nu(COO^-)$ at ≈1410 cm^{-1}, and the C–O vibrations of the epoxy (C–O–C) and C–OH units at ≈1230 cm^{-1}, display evident decreases in their intensity. These facts indicate that a thermal annealing treatment could indeed lead to a removal of the oxygen-containing groups of GO nanosheets, and also the elimination of the carboxylate anions, which are originally generated by the interaction of the $-NH_2$ groups of our cross-linkages and the -COOH groups of GO nanosheets. Together with the facts observed from the UV-vis (Figure S4, Supporting Information) and Raman spectra (Figure S5, Supporting Information), these facts further suggest the successful reduction of the films. On the other hand, as shown in Figure 1, after the thermal annealing treatment, other vibrations associated with the interlayer covalent cross-linkages survive themselves very well in the FT-IR spectra. Accompanied by the observations of the high stability of the films (Supporting Information, Figure S2, panels A2, B2, C2), these facts further confirm that the obtained RGO films could inherit the covalent feature of their parent GO films.

The XPS spectra of our samples were also investigated, as shown in **Figure 3** and Supporting Information, Figures S7,S8. For the originally formulated films before the annealing, their C1s XPS spectra display typical C–C, C–O, C=O, C(O)–O and C–N signals at ≈284.5, 286.5, 287.9, 289.4, and 285.4 eV, respectively.[22b,24] The atom ratio between oxygen and carbon (O/C) is semiquantitatively evaluated to be ≈0.6–0.7. In addition, their N1s XPS spectra display signal of C-N and C-NH_3^+ at ≈400.1 and 401.7 eV,[25] respectively. The atom ratio between nitrogen and carbon (N/C) is estimated to be ≈0.05–0.07. Accompanied by the experimental facts of the FT-IR investigations (Figure 1), these results further indicate the covalent intercalation of our amino-substituted π-conjugated cross-linkages in the as-assembled films, although some of the amino groups of our cross-linkages would also interact with the carboxylic acid groups of GO, resulting in the generation of C–NH_3^+ units in the formulated GO films.

The C1s and N1s XPS spectra of the samples after the thermal annealing were also measured, as shown in Figure 3 and Supporting Information (Figures S7,S8). In these cases, the signals of the oxygen-containing units display an evident decrease compared with those of the original samples before the annealing, wherein the O/C is evaluated to be ≈0.2–0.3.

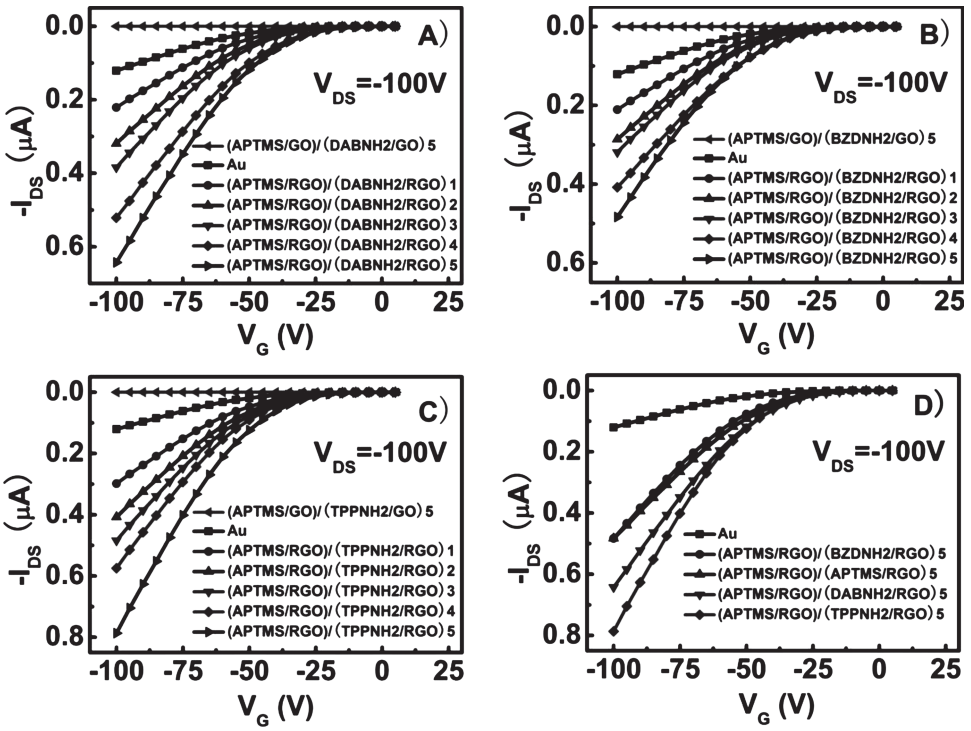

Figure 4. A–C): transfer characteristics of the OFETs based on A) the (APTMS/RGO)/(DABNH2/RGO)N, B) (APTMS/RGO)/(BZDNH2/RGO)N, and C) (APTMS/RGO)/(TPPNH2/RGO)N electrodes. Those using the unreduced GO films, (APTMS/GO)/(DABNH2/GO)5, (APTMS/GO)/(BZDNH2/GO)5, and (APTMS/GO)/(TPPNH2/GO)5, and Au films (40 nm) as electrodes are also presented for comparison. D): a comparison of the transfer characteristics of the devices using (APTMS/RGO)/(APTMS/RGO)5, (APTMS/RGO)/(DABNH2/RGO)5, (APTMS/RGO)/(BZDNH2/RGO)5, (APTMS/RGO)/(TPPNH2/RGO)5 and 40 nm Au films as electrodes. For other comparisons, wherein the number of the bilayers N = 1, 2, 3 and 4, see Figure S10 (Supporting Information).

These values are distinctly lower than those of the parent films before the thermal annealing treatment, solidly indicative of the successful removal of some of the oxygen-containing units and thus the achievement of annealing-induced reduction. On the other hand, the signals relating to N display only slight changes, except that those of C–NH_3^+ at ≈401.7 eV exhibit substantial decreases. This is owing to the thermal reduction-induced elimination of the carboxylic acid groups of GO nanosheets. This could be supported by the FT-IR spectra of the samples, wherein the symmetrical stretching vibrations of carboxylate anion (COO^-) at ≈1410 cm^{-1}, and C=O carbonyl stretching at ≈1730 cm^{-1} display a distinct decrease after the thermal annealing (Figure 1, curves C2, D2, and E2). At the same, it is noteworthy that the N/C is esitmated to be ≈0.04–0.06, which is very close to that of the original unreduced GO films. Accompanied by the information deduced from the FT-IR investigation (Figure 1), and the almost unchanged UV-vis spectra of the RGO films after the ultrasonication treatment (Figure S2, Supporting Information), these present experimental facts further indicate that our RGO films could indeed inherit the covalent features of the originally formulated GO films, which play an important role for their high stability, although the COO^- and the C-NH_3^+ units are greatly removed after the annealing.

To demonstrate the possible advantages of our graphene-based ultrathin films crosslinked by π-conjugated molecules, the formulated samples were integrated as source/drain electrodes into OFETs (Supporting Information, Figure S9) using copper phthalocyanine (CuPc) as the active semiconductor layer, and their performances were measured. Those of the OFETs using (APTMS/RGO)/(APTMS/RGO)N films[9a] or 40 nm Au films as electrodes were also presented for comparison. All of the measurements were carried out in ambient environment at room temperature. The transfer and output characteristics of our devices are shown in **Figure 4**, Figure S10 (Supporting Information), and **Figure 5**, Figures S11–S18 (Supporting Information), respectively. It can be seen from Figure 4 that the OFETs show completely suppressed field-effects when unreduced GO films, (APTMS/GO)/(DABNH2/GO)5, (APTMS/GO)/(BZDNH2/GO)5 and (APTMS/GO)/(TPPNH2/GO)5, are employed as the electrodes. This could be owing to the extremely high resistance of these films, as indicated in **Figure 6**.

In contrast, when Au films or our RGO films are used as electrodes, distinct field-effect behaviors could be observed (Figures 4, 5 and Supporting Information, Figures S10–S18). It is found that the devices based on the RGO electrodes show improved field-effects compared with those of the OFETs based on the traditional Au electrodes. This suggests the high-performances of the devices based on our RGO electrode. It is well established that graphene materials are more compatible with organic semiconductors than the gold films, the contact resistance between the graphene-based materials and organic

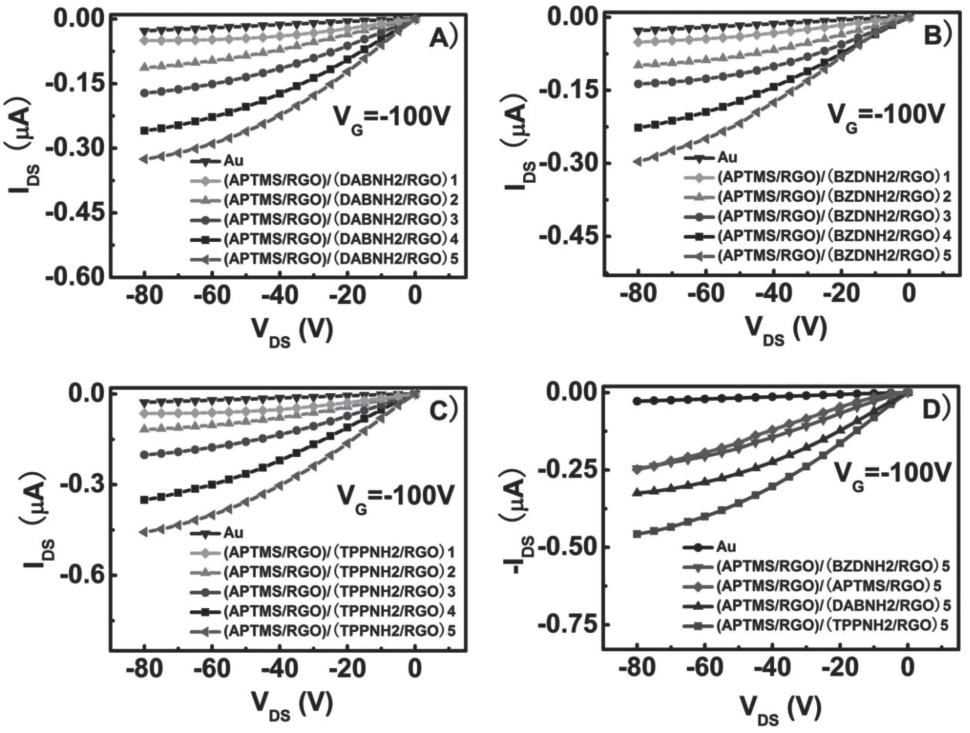

Figure 5. A–C): output characteristics of the OFETs based on A) the (APTMS/RGO)/(DABNH2/RGO)N, B) (APTMS/RGO)/(BZDNH2/RGO)N, and C) (APTMS/RGO)/(TPPNH2/RGO)N electrodes at V_G = –100 V. Those using 40 nm Au films as electrodes are also presented for comparison. See Supporting Information, Figure S11–S13, for those of the devices at V_G = –20, –40, –60, and –80 V. D): a comparison of the output characteristics of the devices using (APTMS/RGO)/(APTMS/RGO)5, (APTMS/RGO)/(DABNH2/RGO)5, (APTMS/RGO)/(BZDNH2/RGO)5, (APTMS/RGO)/(TPPNH2/RGO)5 and 40 nm Au films as electrodes. For other comparisons, wherein the number of the bilayers N = 1, 2, 3, and 4 at V_G = –100 V, see Figure S14 (Supporting Information), while N = 1, 2, 3, 4 and 5 at V_G = –20, –40, –60, and –80 V, see Figures S15–S18 (Supporting Information).

semiconductors might thus be lower than that between Au films and organic semiconductors,[21,26,27] leading to an improved performance of the electronics based on graphene electrodes. This nice compatibility between RGO and organic semiconductors could be explained as the better contact between RGO and organic materials than that between Au and organic materials, especially for such macro-conjugated compound like CuPc, which has a well-known π-conjugated system. This might favor the π–π interactions between our RGO film and the CuPc layer, facilitating a lower contact resistance. To verify this issue in our present case, the contact resistance of our OFETs were investigated by a transfer length method (TLM).[28,29] As shown in **Figure 7**, the experimental results indicate that the contact resistances of our OFETs based on (APTMS/RGO)/(DABNH2/RGO)N, (APTMS/RGO)/(BZDNH2/RGO)N and (APTMS/RGO)/(TPPNH2/RGO)N electrodes are ≈0.08 MΩ cm. These values are almost similar to those of the corresponding devices based on (APTMS/RGO)/(APTMS/RGO)N electrodes,[9a] while distinctly smaller than the ≈2.1 MΩ cm of the devices based on Au electrodes. These facts confirm that the lower contact resistance of our OFETs based on the RGO electrodes plays an important role for their high performances.[21,26,27]

As shown in Figures 4, 5 and Figures S11–S13 (Supporting Information), the performances of our devices based on the RGO electrodes exhibit a distinct improvement with the increase of the number of the bilayers N. Meanwhile, it can be seen from Figure 4D,5D, and Figures S10,S14–S18 (Supporting Information) that the devices using our (APTMS/RGO)/(DABNH2/RGO)N films as the electrodes display improved field-effects compared with the corresponding devices based on the (APTMS/RGO)/(APTMS/RGO)N electrodes of the similar number of bilayers N. Note that the OFETs based on these two kinds of electrodes both have a very close contact resistance (**Figure 7**).[9a] This indicates that the contact resistance is not responsible for their different electrical behaviors. Accordingly, we propose that the distinctly improved performance of the (APTMS/RGO)/(DABNH2/RGO)N electrodes might be stemmed from the intercalation of the π-conjugated phenyl units between the RGO interlayers, since it is known that the electronically active delocalized electrons of π-conjugated molecules could provide conductive pathways along their molecular skeleton.[10,30a] To verify this, the conductance of our (APTMS/RGO)/(DABNH2/RGO)N electrodes were measured.[31] As shown in Figure 6A, when the number of bilayers of the (APTMS/RGO)/(DABNH2/RGO)N films increases, their conductance increases correspondingly. Consequently, the performance of the corresponding OFETs increases with the increasing of the number of bilayers N (Figures 4A,5A and Figure S11, Supporting Information). Meanwhile, it can be seen that compared with the corresponding (APTMS/RGO)/(APTMS/RGO)N films,[9a] our (APTMS/RGO)/(DABNH2/RGO)N electrodes display a higher conductance (Figure 6D).

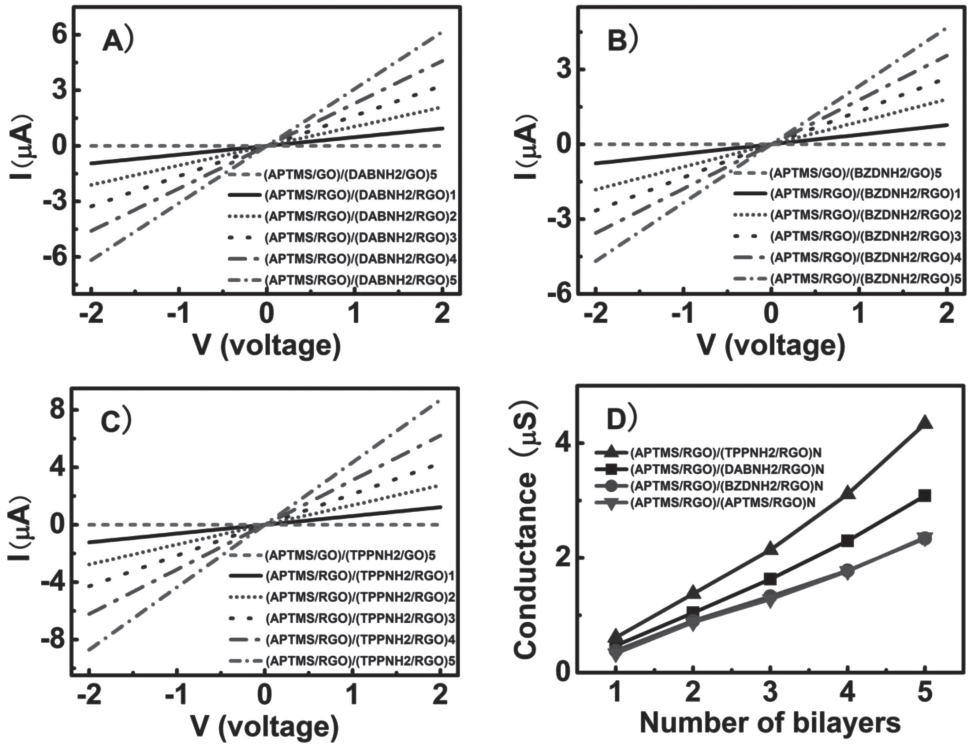

Figure 6. Current-voltage (*I–V*) curves of A) the (APTMS/RGO)/(DABNH2/RGO)N, B) (APTMS/RGO)/(BZDNH2/RGO)N, and C) (APTMS/RGO)/(TPPNH2/RGO)N films. The results of the unreduced GO films, (APTMS/GO)/(DABNH2/GO)5, (APTMS/GO)/(BZDNH2/GO)5, and (APTMS/GO)/(TPPNH2/GO)5, are also presented in the corresponding panels for comparison. D) The conductance of these films versus the number of bilayers *N*, wherein those of the (APTMS/RGO)/(APTMS/RGO)N films are also collected in the same panel for comparison. These *I–V* curves were measured with $V_G = 0$ V.

These facts confirm that the phenyl units of DABNH2 molecules intercalated between the RGO interlayers could indeed work as electronically active species[30a] for the improvement of the conductance of the LBL films, leading to an improved performance of the corresponding devices.

It thus could be expected that improved electrical performances might also be realized in the nanodevices using (APTMS/RGO)/(BZDNH2/RGO)N as electrodes, since BZDNH2 molecules are also π-conjugated species. Along this line of thought, the transfer and output characteristics of the integrated devices were measured, as shown in Figures 4B, 5B and Figure S12 (Supporting Information). Surprisingly, the results indicate that compared with the corresponding devices based on the (APTMS/RGO)/(DABNH2/RGO)N electrodes of the similar number of bilayers *N*, those using (APTMS/RGO)/(BZDNH2/RGO)N as electrodes display decreased performances, while they exhibit roughly similar electrical behaviors compared with the corresponding OFETs based on (APTMS/RGO)/(APTMS/RGO)N electrodes (Figures 4D, 5D, and Figures S10,S14–S18, Supporting Information). Considering

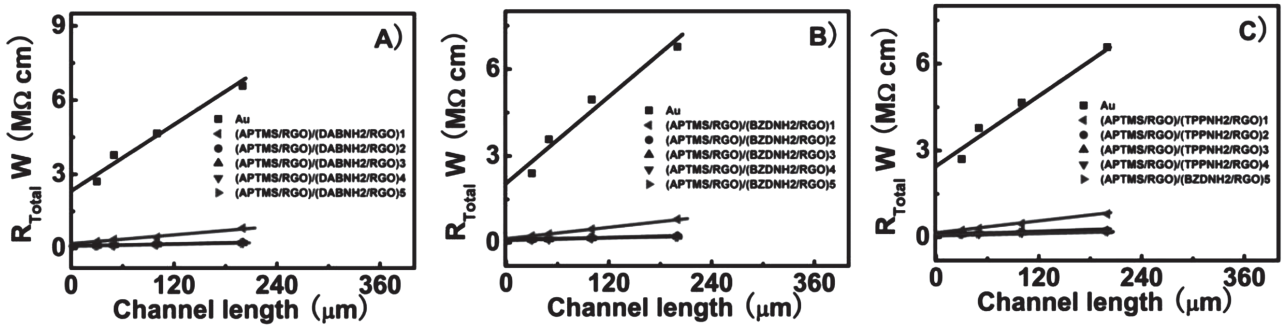

Figure 7. Channel width-normalized R_{Total} of the OFETs using A) (APTMS/RGO)/(DABNH2/RGO)N, B) (APTMS/RGO)/(BZDNH2/RGO)N, and C) (APTMS/RGO)/(TPPNH2/RGO)N films as electrodes. The results of the devices using 40 nm Au films as electrodes are also shown for comparison.

the fact that the OFETs based on these RGO electrodes have a similar contact resistance (Figure 7),[9a] the abnormal performances of the (APTMS/RGO)/(BZDNH2/RGO)N electrodes might be attributed to the conductance of (APTMS/RGO)/(BZDNH2/RGO)N films. This could be experimentally supported by the conductance measurements (Figure 6B,D), wherein it is found that the (APTMS/RGO)/(BZDNH2/RGO)N films display approximately similar conductance as the corresponding (APTMS/RGO)/(APTMS/RGO)N electrodes, while smaller conductance compared with the corresponding (APTMS/RGO)/(DABNH2/RGO)N electrodes. As it is known that different from DABNH2 molecules, which have a planar π-conjugated phenyl unit, a torsion angle of ≈32°–42° exists between the planes of the two phenyl units of biphenyl.[30b] It has been proved that this nonplanarity makes biphenyl less conductive than phenyl.[30a] Consequently, it could be suggested that the nonplanarity of the BZDNH2 molecules contributes much[30a] to the abnormal electrical performances of the devices based on the (APTMS/RGO)/(BZDNH2/RGO)N electrodes.

It thus could be seen that the intercalation of cross-linkages of different π-conjugated systems into the interlayers of our covalently bridged RGO films could arouse interesting electrical behaviors. As known, as one of the most distinguished π-conjugated molecules, porphyrins, which are composed of four pyrrole rings bridged together via the α position through four methine groups, have recently received much attentions as electronically active components for diverse nanodevices.[10d,32] This is resulted from their unique planar as well as rigid molecular geometry and aromatic electronic feature delocalized over their molecular frame, which favor an effective charge carrier transport and thus high-performance nanoelectronics.[10d,32] As shown in Figures 4C, 5C and Figure S13 (Supporting Information), the transfer and output characteristics of the OFETs using (APTMS/RGO)/(TPPNH2/RGO)N films as the source/drain electrodes are also investigated. It can be seen that compared with the corresponding OFETs using (APTMS/RGO)/(APTMS/RGO)N, (APTMS/RGO)/(DABNH2/RGO)N and (APTMS/RGO)/(BZDNH2/RGO)N films of the similar number of bilayers *N* as the electrodes, those based on (APTMS/RGO)/(TPPNH2/RGO)N electrodes display evidently improved performances (Figure 4D, 5D, and Figures S10,S14–S18, Supporting Information).

On one hand, as shown in Figure 7, all of our devices based on RGO electrodes display approximately similar contact resistance. On the other hand, as suggested by the conductance measurements shown in Figure 6C, the (APTMS/RGO)/(TPPNH2/RGO)N films, using TPPNH2 as the cross-linkages, display distinctly larger conductance compared with the corresponding films of (APTMS/RGO)/(APTMS/RGO)N, (APTMS/RGO)/(DABNH2/RGO)N and (APTMS/RGO)/(BZDNH2/RGO)N, which use ATPMS, DABNH2, and BZDNH2 as the cross-linkages, respectively (Figure 6D). Accordingly, these facts confirm that the improved performance of the OFETs based on the (APTMS/RGO)/(TPPNH2/RGO)N electrodes is, to a great extent, owing to the effective conjugation system of porphyrins,[10d] which favors an efficient charge carrier transport.

3. Conclusion

In summary, we have shown that amino-substituted π-conjugated molecules, DABNH2, BZDNH2, and TPPNH2, could work as cross-linkages for a controllable assembly of graphene-based ultrathin films. The intercalation of these molecules into graphene interlayers endows our films with excellent stability, controllable thickness and tunable electrical behaviors. The OFETs based on the (APTMS/RGO)/(BZDNH2/RGO)N electrodes exhibit almost similar electrical performances to those of the devices based on the (APTMS/RGO)/(APTMS/RGO)N electrodes, which are crosslinked by non-π-conjugated compound APTMS. Improved performances could be realized when DABNH2 is intercalated, while further enhanced performances are achieved when RGO films crosslinked by TPPNH2 are used. Here, the function of the cross-linkage is dual, that is, it could play a crucial role for the excellent stability and controlled thickness of the electrodes and, more importantly, for their tunable performances. This makes our graphene-based films have bright application futures. We believe that our new protocol will provide high-quality graphene-based films not only for high-performance next generation organic nanoelectronics, but also for the other desired motives by using elaborately-designed covalent cross-linkages of desired functions.

4. Experimental Section

Materials and Substrates: 1,4-diaminobenzene (DABNH2, Aldrich, 99%,), benzidine (BZDNH2, Alfa Aesar, 98%), and 5,10,15,20-tetrakis (4-aminophenyl)-21H,23H-porphine (TPPNH2, TCI, 95%), (3-aminopropyl) trimethoxysilane (APTMS, Alfa Aesar, 97%), which were used as covalent cross-linkages for the fabrication of LBL films were used as received without further treatments. Graphite power (325 mesh, 99.9995%), which was used for the synthesis of GO nanosheets was purchased from Alfa Aesar. Copper phthalocyanine (CuPc) was purchased from the Aldrich Company and purified by gradient sublimation twice before use. GO nanosheets were synthesized via a chemical exfoliation of the graphite powder using a modified Hummers method.[33] The lateral size of the as-formulated GO nanosheets was ≈300 nm–1 μm, and their thickness was ≈0.8 nm.[33c]

To fabricate LBL films, quartz plates, silicon slides, and N-doped silicon wafer with a 500 nm SiO_2 layer (SiO_2/Si) were cleaned and hydroxylated by immersing in a piranha solution (H_2SO_4:H_2O_2 = 7:3, by volume) at 80 °C for 1 h. Before used, these substrates were rinsed and ultrasonicated thoroughly with Milli-Q water and then dried under nitrogen flow. Silicon slides were employed as the solid supports for the measurments of FT-IR, XPS and Raman spectra. SiO_2/Si wafers were used as the solid supports for AFM measurements and for the investigation of the electrical performances of the OFETs. For the measurement of UV-vis and XRD spectra, quartz plates were used as the substrates.

Assembly of GO Films by Means of an LBL Protocol, and the Thermal Annealing Induced Reduction of the Samples: Before the assembly of the LBL films using our π-conjugated compounds as covalent cross-linkages, a (ATPMS/GO) sublayer was covalently anchored on the solid supports using APTMS as covalent anchors.[9a] The obtained (APTMS/GO) films were subsequently used as the sublayers for the construction of (APTMS/GO)/(DABNH2/GO)N, (APTMS/GO)/(BZDNH2/GO)N and (APTMS/GO)/(TPPNH2/GO)N multilayer LBL films (Scheme 1). Experimentally, the (ATPMS/GO) sublayer-modified substrates were immersed in a DMSO solution of our π-conjugated compounds for 60 min at 30 °C for DABNH2 and BZDNH2, and at 70 °C for TPPNH2, respectively. After that, the samples were rinsed and ultrasonicated thoroughly in DMSO

for 15 min, wherein the ultrasonication performances were carried out repeatedly three times. Then, the resultant samples were dried under nitrogen flow. Subsquently, the as-prepared samples were immersed in an an aqueous dispersion of GO nanosheets for 60 min, after which the formulated films were rinsed and ultrasonicated thoroughly in water for 15 min, which was also performed repeatedly three times. Multilayered GO LBL films with desired number of bilayers *N* could thus be formulated by repeating the above operations alternately and consecutively, as shown in Scheme 1. The fabricated films could be used for various characterizations or for the fabrication of nanoelectronics.

To obtain RGO films, the above-fabricated GO LBL films were thermally annealed for 16 h at 180 °C under a flow of argon gas.[22b,25] The thermal annealing was performed in a tube oven (Lindberg/BlueM3-zone tube oven, Blue-M, White Deer, PA). After the annealing treatments, the samples were subjected to various characterizations, measurements, or to the fabrication of OFETs.

Stability of the Formulated Graphene-Based Films: The formulated covalently crosslinked GO or RGO films were ultrasonicated in Milli-Q water (250 W, 40 kHz) for 5 h with the water bath temperature maintained at *ca.* 20 °C. The ultrasonication operations were carried out using an ultrasonic cleaner (KQ250B, 250 W, 40 kHz, Kunshan, Ultrasonic Instruments Co. Ltd, Kunshan, China). After such ultrasonication treatments, the samples were washed with water thoroughly and dried under nitrogen flow. Then, the UV-vis spectra of the obtained sample were measured.

Fabrication of OFETs Using Our π-conjugated Molecules Crosslinked Films as Source/Drain Electrodes: To obtain source/drain electrodes, a 40 nm aluminum film was evaporated onto our graphene-based films under vacuum by using a copper grid, which has a channel length of 26 μm and width of 200 μm, as a mask. The uncovered area of the graphene films could be eliminated via an oxygen plasma cleaner (the clear operation was performed for 5 min with 20 sccm O_2 flow and 300 W rf power). Subsequently, patterned graphene-based electrodes were produced via a wet etching of the aluminum film by immersing the samples in a 10% HNO_3 solution for 30 min at 50 °C.[27a] Experimentally, we found that the properties of our samples after the patterning displayed negligible changes. This was resulted from the existence of the covalent bonds between the interlayers, which made our LBL films have an excellent stability. For the integration of OFETs, a CuPc film of 40 nm, which serve as active layer, was evaporated on the patterned electrodes under vacuum.

Apparatus, Characterizations, and Measurements: JASCO IR-660 and JASCO UV-550 spectrometers were used for the measurements of the FT-IR and UV-vis spectra, respectively. Raman spectra were investigated on a Renishaw inVia plus Raman microscope using a 514.5 nm argon ion laser. X-Ray diffraction (XRD) measurements were performed on a PANalytical X'Pert PRO instrument with Cu Kα radiation. The X-ray photoelectron spectroscopy (XPS) was measured on an ESCALab220i-XL electron spectrometer from VG Scientific using 300 W Al Kα radiation, wherein the binding energies were referenced to the C 1s line at 284.8 eV from adventitious carbon. The AFM images, without any image processing except flattening, were recorded by using the tapping mode on a Digital Instrument Nanoscope IIIa Multimode system (Santa Barbara, CA) with a silicon cantilever. The microscopic optical images of patterned electrodes were recorded by an optical microscopy (Zeiss). The performances of our OFETs in terms of the transfer and output characteristics, and the *I–V* characteristics of our graphene-based films, were investigated with a Keithley 4200 SCS and a Micromanipulator 6150 probe station in a clean and shielded box. All of the above-mentioned characterizations and measurements were performed in the ambient environment at room temperature except noted.

The channel width-normalized contact resistances ($R_C W$) of our devices were measured on Keithley system by a transfer length method (TLM).[28,29] The R_{Total} was deduced from the inverse slope of the linear regime of each *I–V* curve. The contact resistances were estimated using the TLM with a varying channel length of 30, 50, 100, 200 μm, and a channel width of 500 μm. A gate bias of –60 V was employed for the measurements, and the contact resistance of the devices was extracted from the $L = 0$ intersection of the resistances.

Supporting Information

Supporting Information is available from the Wiley Online Library or from the author.

Acknowledgment

This work was supported financially by the National Natural Science Foundation of China (21372225, 20773141, 20873159, 21021003, and 91027042), the National Key Basic Research Project of China (2011CB932301 and 2013CB834504), and the Chinese Academy of Sciences (1731300500015). The authors are grateful to Prof. Fen Liu from the Institute of Chemistry, Chinese Academy of Sciences, for her profound discussions concerning the analyses of the XPS spectra. P.C. thanks Zhengzhou University for the "Talent Project of Distinguished Professor".

Received: June 25, 2013
Revised: July 24, 2013
Published online: September 3, 2013

[1] a) X. Huang, X. Qi, F. Boey, H. Zhang, *Chem. Soc. Rev.* **2012**, *41*, 666; b) Y. Zhu, S. Murali, W. Cai, X. Li, J. W. Suk, J. R. Potts, R. S. Ruoff, *Adv. Mater.* **2010**, *22*, 3906; c) D. Wu, F. Zhang, H. Liang, X. Feng, *Chem. Soc. Rev.* **2012**, *41*, 6160; d) G. Eda, Y.-Y. Lin, S. Miller, C.-W. Chen, W.-F. Su, M. Chhowalla, *Appl. Phys. Lett.* **2008**, *92*, 233305.

[2] a) H. Wang, H. Dai, *Chem. Soc. Rev.* **2013**, *42*, 3088; b) H. Bai, C. Li, G. Shi, *Adv. Mater.* **2011**, *23*, 1089; c) Q. He, S. Wu, Z. Yin, H. Zhang, *Chem. Sci.* **2012**, *3*, 1764; d) S. Pang, Y. Hernandez, X. Feng, K. Müllen, *Adv. Mater.* **2011**, *23*, 2779.

[3] a) Z. Yin, S. Sun, T. Salim, S. Wu, X. Huang, Q. He, Y. M. Lam, H. Zhang, *ACS Nano* **2010**, *4*, 5263; b) X. Wang, L. Zhi, K. Müllen, *Nano Lett.* **2008**, *8*, 323; c) Z. Yin, S. Wu, X. Zhou, X. Huang, Q. Zhang, F. Boey, H. Zhang, *Small* **2010**, *6*, 307; d) J. Wu, M. Agrawal, H. A. Becerril, Z. Bao, Z. Liu, Y. Chen, P. Peumans, *ACS Nano* **2010**, *4*, 43.

[4] Reviews, see: M. Yang, Y. Hou, N. A. Kotov, *Nano Today* **2012**, *7*, 430, and the references therein.

[5] a) H. A. Becerril, R. M. Stoltenberg, M. L. Tang, M. E. Roberts, Z. Liu, Y. Chen, D. H. Kim, B.-L. Lee, S. Lee, Z. Bao, *ACS Nano* **2010**, *4*, 6343; b) K. K. Manga, Y. Zhou, Y. Yan, K. P. Loh, *Adv. Funct. Mater.* **2009**, *19*, 3638; c) J. Kim, L. J. Cote, J. Huang, *Acc. Chem. Res.* **2012**, *45*, 1356; d) L. J. Cote, F. Kim, J. Huang, *J. Am. Chem. Soc.* **2009**, *131*, 1043.

[6] a) X. Li, G. Zhang, X. Bai, X. Sun, X. Wang, E. Wang, H. Dai, *Nat. Nanotechnol.* **2008**, *3*, 538; b) Z.-S. Wu, S. Pei, W. Ren, D. Tang, L. Gao, B. Liu, F. Li, C. Liu, H.-M. Cheng, *Adv. Mater.* **2009**, *21*, 1756; c) H. Li, S. Pang, S. Wu, X. Feng, K. Mullen, C. Bubeck, *J. Am. Chem. Soc.* **2011**, *133*, 9423; d) S. Gilje, S. Han, M. Wang, K. L. Wang, R. B. Kaner, *Nano Lett.* **2007**, *7*, 3394; e) K. Sheng, H. Bai, Y. Sun, C. Li, G. Shi, *Polymer* **2011**, *52*, 5567; f) S. Wang, P. K. Ang, Z. Wang, A. L. L. Tang, J. T. L. Thong, K. P. Loh, *Nano Lett.* **2010**, *10*, 92.

[7] a) J. R. Hauptmann, T. Li, S. Petersen, J. Nygård, P. Hedegård, T. Bjørnholm, B. W. Laursen, K. Nørgaard, *Phys. Chem. Chem. Phys.* **2012**, *14*, 14277; b) O. C. Compton, D. A. Dikin, K. W. Putz, L. C. Brinson, S. T. Nguyen, *Adv. Mater.* **2010**, *22*, 892; c) H. Y. Jeong, J. Y. Kim, J. W. Kim, J. O. Hwang, J.-E. Kim, J. Y. Lee, T. H. Yoon, B. J. Cho, S. O. Kim, R. S. Ruoff, S.-Y. Choi, *Nano Lett.* **2010**, *10*, 4381; d) V. Lee, L. Whittaker, C. Jaye, K. M. Baroudi, D. A. Fischer, S. Banerjee, *Chem. Mater.* **2009**, *21*, 3905; e) T. N. Lambert,

C. A. Chavez, N. S. Bell, C. M. Washburn, D. R. Wheeler, M. T. Brumbach, *Nanoscale* **2011**, *3*, 188; f) E. Ou, X. Zhang, Z. Chen, Y. Zhan, Y. Du, G. Zhang, Y. Xiang, Y. Xiong, W. Xu, *Chem. Eur. J.* **2011**, *17*, 8789.

[8] a) Q. Ji, I. Honma, S.-M. Paek, M. Akada, J. P. Hill, A. Vinu, K. Ariga, *Angew. Chem. Int. Ed.* **2010**, *49*, 9737; b) H.-B. Yao, L.-H. Wu, C.-H. Cui, H.-Y. Fang, S.-H. Yu, *J. Mater. Chem.* **2010**, *20*, 5190.

[9] a) X. Ou, L. Jiang, P. Chen, M. Zhu, W. Hu, M. Liu, J. Zhu, H. Ju, *Adv. Funct. Mater.* **2013**, *23*, 2422; b) K. Ariga, J. P. Hill, Q. Ji, *Phys. Chem. Chem. Phys.* **2007**, *9*, 2319; c) X. Zhang, H. Chen, H. Zhang, *Chem. Commun.* **2007**, 1395; d) D. E. Bergbreiter, K.-S. Liao, *Soft Matter* **2009**, *5*, 23.

[10] a) S. Varghese, S. Das, *J. Phys. Chem. Lett.* **2011**, *2*, 863; b) C. Wang, H. Dong, W. Hu, Y. Liu, D. Zhu, *Chem. Rev.* **2012**, *112*, 2208; c) B.-K. An, J. Gierschner, S. Y. Park, *Acc. Chem. Res.* **2012**, *45*, 544; d) C. Wang, H. Dong, W. Hu, Y. Liu, D. Zhu, *Chem. Rev.* **2012**, *112*, 2208.

[11] a) D.-D. Zhang, S.-Z. Zua, B.-H. Han, *Carbon* **2009**, *47*, 2993; b) Y. Lin, J. Jin, M. Song, *J. Mater. Chem.* **2011**, *21*, 3455; c) H. Yang, F. Li, C. Shan, D. Han, Q. Zhang, L. Niu, A. Ivaska, *J. Mater. Chem.* **2009**, *19*, 4632; d) J. Ou, J. Wang, S. Liu, B. Mu, J. Ren, H. Wang, S. Yang, *Langmuir* **2010**, *26*, 15830.

[12] a) A. V. Murugan, T. Muraliganth, A. Manthiram, *Chem. Mater.* **2009**, *21*, 5004; b) M. Jahan, Q. Bao, J.-X. Yang, K. P. Loh, *J. Am. Chem. Soc.* **2010**, *132*, 14487; c) X. Tu, S. Luo, G. Chen, J. Li, *Chem. Eur. J.* **2012**, *18*, 14359.

[13] a) S. Bernt, V. Guillerm, C. Serre, N. Stock, *Chem. Commun.* **2011**, *47*, 2838; b) G. Sun, C.-C. Chu, *ACS Nano* **2009**, *3*, 1176; c) C.-H. Wang, W.-T. Wang, G.-H. Hsiue, *Biomaterials* **2009**, *30*, 3352; d) S. S. Mahapatra, S. K. Yadav, H. J. Yoo, J. W. Cho, *J. Mater. Chem.* **2011**, *21*, 7686.

[14] a) A. Politano, A. R. Marino, V. Formoso, G. Chiarello, *AIP Adv.* **2011**, *1*, 042130; b) H. Yan, F. Xia, W. Zhu, M. Freitag, C. Dimitrakopoulos, A. A. Bol, G. Tulevski, P. Avouris, *ACS Nano* **2011**, *5*, 9854.

[15] a) A. Politano, G. Chiarello, *Appl. Phys. Lett.* **2013**, *102*, 201608; b) A. S. Barnard, I. K. Snook, *Carbon* **2010**, *48*, 981; c) D. C. Elias, R. R. Nair, T. M. G. Mohiuddin, S. V. Morozov, P. Blake, M. P. Halsall, A. C. Ferrari, D. W. Boukhvalov, M. I. Katsnelson, A. K. Geim, K. S. Novoselov, *Science* **2009**, *323*, 610; d) A. Politano, G. Chiarello, *Nanoscale* **2013**, *ASAP*, DOI: 10.1039/c3nr02027d; e) A. Politano, A. R. Marino, G. Chiarello, *Phys. Rev. B* **2012**, *86*, 085420.

[16] a) C. S. Harris, M. A. Ratner, D. F. Shriver, *Macromolecules* **1987**, *20*, 1778; b) Ma. I. Coahuila Hernández, M. A. García Sánchez, A. M. Soto Estrada, A. Campero, *J. Sol-Gel Sci. Technol.* **2006**, *37*, 117.

[17] a) X. Huang, S. Jiang, M. Liu, *J. Phys. Chem. B* **2005**, *109*, 114; b) L. M. Bronstein, X. Huang, J. Retrum, A. Schmucker, M. Pink, B. D. Stein, B. Dragnea, *Chem. Mater.* **2007**, *19*, 3624.

[18] L.-H. Liu, M. Yan, *Nano Lett.* **2009**, *9*, 3375.

[19] a) M. J. McAllister, J.-L. Li, D. H. Adamson, H. C. Schniepp, A. A. Abdala, J. Liu, M. Herrera-Alonso, D. L. Milius, R. Car, R. K. Prud'homme, I. A. Aksay, *Chem. Mater.* **2007**, *19*, 4396; b) H. C. Schniepp, J.-L. Li, M. J. McAllister, H. Sai, M. Herrera-Alonso, D. H. Adamson, R. K. Prud'homme, R. Car, D. A. Saville, I. A. Aksay, *J. Phys. Chem. B* **2006**, *110*, 8535; c) O. Akhavan, E. Ghaderi, *J. Phys. Chem. C* **2009**, *113*, 20214.

[20] D. Li, M. B. Müller, S. Gilje, R. B. Kaner, G. G. Wallace, *Nat. Nanotechnol.* **2008**, *3*, 101.

[21] P. Yao, P. Chen, L. Jiang, H. Zhao, H. Zhu, D. Zhou, W. Hu, B.-H. Han, M. Liu, *Adv. Mater.* **2010**, *22*, 5008.

[22] a) D. Yang, A. Velamakanni, G. Bozoklu, S. Park, M. Stoller, R. D. Piner, S. Stankovich, I. Jung, D. A. Field, C. A. Ventrice Jr., R. S. Ruoff, *Carbon* **2009**, *47*, 145; b) S. Stankovich, D. A. Dikin, R. D. Piner, K. A. Kohlhaas, A. Kleinhammes, Y. Jia, Y. Wu, S. T. Nguyen, R. S. Ruoff, *Carbon* **2007**, *45*, 1558; c) Z.-S. Wu, W. Ren, L. Gao, J. Zhao, Z. Chen, B. Liu, D. Tang, B. Yu, C. Jiang, H.-M. Cheng, *ACS Nano* **2009**, *3*, 411; d) Z. H. Ni, H. M. Wang, Y. Ma, J. Kasim, Y. H. Wu, Z. X. Shen, *ACS Nano* **2008**, *2*, 1033.

[23] a) Q. Zheng, W. H. Ip, X. Lin, N. Yousefi, K. K. Yeung, Z. Li, J.-K. Kim, *ACS Nano* **2011**, *5*, 6039; b) D. W. Lee, T.-K. Hong, D. Kang, J. Lee, M. Heo, J. Y. Kim, B.-S. Kim, H. S. Shin, *J. Mater. Chem.* **2011**, *21*, 3438; c) Q. B. Zheng, M. M. Gudarzi, S. J. Wang, Y. Geng, Z. Li, J.-K. Kim, *Carbon* **2011**, *49*, 2905.

[24] a) X.-Z. Tang, W. Li, Z.-Z. Yu, M. A. Rafiee, J. Rafiee, F. Yavari, N. Koratkar, *Carbon* **2011**, *49*, 1258; b) Y. He, H. Cui, *J. Mater. Chem.* **2012**, *22*, 9086.

[25] O. C. Compton, D. A. Dikin, K. W. Putz, L. C. Brinson, S. T. Nguyen, *Adv. Mater.* **2010**, *22*, 892.

[26] C.-A. Di, D. Wei, G. Yu, Y. Liu, Y. Guo, D. Zhu, *Adv. Mater.* **2008**, *20*, 3289.

[27] a) S. Pang, H. N. Tsao, X. Feng, K. Müllen, *Adv. Mater.* **2009**, *21*, 3488; b) C.-G. Lee, S. Park, R. S Ruoff, A. Dodabalapur, *Appl. Phys. Lett.* **2009**, *95*, 023304; c) Y. Cao, S. Liu, Q. Shen, K. Yan, P. Li, J. Xu, D. Yu, M. L. Steigerwald, C. Nuckolls, Z. Liu, X. Guo, *Adv. Funct. Mater.* **2009**, *19*, 2743.

[28] W. H. Lee, J. Park, S. H. Sim, S. Lim, K. S. Kim, B. H. Hong, K. Cho, *J. Am. Chem. Soc.* **2011**, *133*, 4447.

[29] a) F. Xia, V. Perebeinos, Y.-M. Lin, Y. Wu, P. Avouris, *Nat. Nanotechnol.* **2011**, *6*, 179; b) A. Venugopal, L. Colombo, E. M. Vogel, *Appl. Phys. Lett.* **2010**, *96*, 013512.

[30] a) L. Venkataraman, J. E. Klare, C. Nuckolls, M. S. Hybertsen, M. L. Steigerwald, *Nature* **2006**, *442*, 904; b) J. L. Brédas, G. B. Street, B. Thémans, J. M. André, *J. Chem. Phys.* **1985**, *83*, 1323.

[31] Considering the dimension of (APTMS/GO) /(DABNH2/GO) N, their conductivity was estimated to be ≈24.9, 37.9, 44.6, 50.5, and 55.7 S m^{-1}, when *N* was 1, 2, 3, 4 and 5, respectively. For (APTMS/RGO) /(BZDNH2/RGO) N and (APTMS/RGO)/(TPPNH2/RGO) N, the corresponding results were 17.4, 26.7, 29.0, 30.8, 33.4 S m^{-1}, and 22.5, 31.0, 34.9, 40.2, 45.1 S m^{-1}, respectively. Conductivities with nice reproducibility were obtained for our RGO LBL films of the same cross-linkage and *N*. The conductivity of the conventional RGO films, which were prepared by a spin coating and a subsequent thermal annealing induced reduction, was estimated to be ≈50–300 S m^{-1}. This is larger than that of our RGO LBL films. In this case, there are no cross-linkages between the RGO sheets, leading to a smaller interlayer distance and thus a higher conductivity. However, owing to the inhomogeneity and uncontrolled thickness of the spin coating films, their conductivity displays poor reproducibility.

[32] a) B. A. Friesen, B. Wiggins, J. L. McHale, U. Mazur, K. W. Hipps, *J. Am. Chem. Soc.* **2010**, *132*, 8554; b) S. Egger, A. Ilie, S. Machida, T. Nakayama, *Nano Lett.* **2007**, *7*, 3399; c) A. D. Schwab, D. E. Smith, B. Bond-Watts, D. E. Johnston, J. Hone, A. T. Johnson, J. C. De Paula, W. F. Smith, *Nano Lett.* **2004**, *4*, 1261.

[33] a) W. S. Hummers, R. E. Offeman, *J. Am. Chem. Soc.* **1958**, *80*, 1339; b) P. Guo, P. Chen, M. Liu, *ACS Appl. Mater. Interfaces* **2013**, *5*, 5336; c) M. Zhu, P. Chen, M. Liu, *Langmuir* **2013**, *29*, 9259; d) M. Zhu, P. Chen, M. Liu, *ACS Nano* **2011**, *5*, 4529.